

Long-term CCD Photometry and Physical Properties of the sdB+M Eclipsing System 2M 1533+3759

Jae Woo Lee^{1,2}, Jae-Hyuck Youn¹, Kyeongsoo Hong¹, and Wonyong Han^{1,2}

¹*Korea Astronomy and Space Science Institute, Daejeon 34055, Korea*

²*Astronomy and Space Science Major, Korea University of Science and Technology, Daejeon 34113, Korea*

jwlee@kasi.re.kr, jhyoon@kasi.re.kr, kshong@kasi.re.kr, whan@kasi.re.kr

ABSTRACT

New CCD photometry of seven successive years from 2010 is presented for the HW Vir-type eclipsing binary 2M 1533+3759. Using the *VI* light curves together with the radial-velocity data given by For et al. (2010), we determined the absolute parameters of each component to be $M_1 = 0.442 \pm 0.012 M_\odot$, $M_2 = 0.124 \pm 0.005 M_\odot$, $R_1 = 0.172 \pm 0.002 R_\odot$, $R_2 = 0.157 \pm 0.002 R_\odot$, $L_1 = 19.4 \pm 1.4 L_\odot$, and $L_2 = 0.002 \pm 0.002 L_\odot$. These indicate that 2M 1533+3759 is a detached system consisting of a normal sdB primary and an M7 dwarf companion. Detailed analyses of 377 minimum epochs, including our 111 timings, showed that the orbital period of the system remains constant during the past 12 yrs. Inspecting both types of minima, we found a delay of 3.9 ± 1.0 s in the arrival times of the secondary eclipses relative to the primary eclipse times. This delay is in satisfactory agreement with the predicted Rømer delay of 2.7 ± 1.4 s and the result is the second measurement in sdB+M eclipsing binaries. The time shift of the secondary eclipse can be explained by some combination of the Rømer delay and a non-zero eccentricity. Then, the binary star would have a very small eccentricity of $e \cos \omega \simeq 0.0001$.

Subject headings: binaries: close — binaries: eclipsing — stars: fundamental parameters — stars: individual (2M 1533+3759) — subdwarfs

1. INTRODUCTION

Subdwarf B (sdB) stars are a class of hot ($T_{\text{eff}} = 22,000\text{--}40,000$ K) and compact ($\log g = 5.0\text{--}6.2$) stars with helium burning cores and hydrogen envelopes too thin to sustain hydrogen shell burning (Heber 2016). In the Hertzsprung-Russell diagram, they are located between the upper main sequence and the white dwarf sequence, also known as the so-called extreme horizontal branch. Recent studies have indicated that about half of the sdB stars are in close binaries with short periods of $P < 10$ d (Maxted et al. 2001; Copperwheat et al. 2011), which are thought to be the products of common envelope evolution (Paczynski 1976; Han et al. 2003). The HW

Vir-type stars, showing a striking reflection effect in light curves, are binary systems with orbital periods of 2–5 h and very low-mass companions (main sequence or brown dwarf). These binaries play an important role in establishing the mass distribution of the sdB stars, which is the key to understand their evolution. The mean mass of sdB stars derived from the binary modeling is $0.471 M_{\odot}$, and it is in good agreement with $0.470 M_{\odot}$ obtained from the asteroseismology of pulsating stars (Fontaine et al. 2012).

Because the HW Vir systems are very short-period binaries with sharp eclipses and there are no peculiar light variations with time, we can measure the mid-eclipse times with timing accuracies of a few seconds from their light curves. The timing measurements are useful for understanding various astrophysical phenomena of binary stars (cf. Kreiner et al. 2001). The presence of a circumbinary object orbiting a binary can cause a sinusoidal variation due to the light-travel-time (LTT) effect (Irwin 1952, 1959) in eclipse timing $O-C$ residuals, which are the differences between the observed (O) and the calculated (C) minima. If the timings with accuracies better than ~ 10 s are enough to investigate the binary’s period behavior, we can detect substellar-mass circumbinary companions such as planets and brown dwarfs (Ribas 2006; Lee et al. 2009a). Zorotovic & Schreiber (2013) indicated that about 38 % of the HW Vir binaries display orbital period changes that could be produced by substellar companions. Such systems are of great interest because they offer significant information about the formation and evolution of the post common-envelope binaries and their circumbinary objects.

In order to look for substellar companions around the HW Vir binaries and to understand their physical properties, we choose 2M 1533+3759 (NSVS 07826147; 2MASS J15334944+3759282; $V = +12.96$). The program target was discovered by Kelley & Shaw (2007) to be a potential sdB binary with an orbital period of about 3.88 h and a narrow eclipse width. For et al. (2010) obtained the $BVRI$ light curves and single-lined radial-velocity (RV) data. From separate analyses of the two datasets, they reported that the eclipsing binary is a detached system with a mass ratio of $q = 0.301$, an inclination of $i = 86.6$ deg, a surface gravity of $\log g_1 = 5.58$, and effective temperatures of $T_1 = 29,230$ K and $T_2 = 3100$ K. Individual masses and radii of the sdB primary and cool secondary were determined to be $M_1 = 0.376 M_{\odot}$, $M_2 = 0.113 M_{\odot}$, $R_1 = 0.166 R_{\odot}$, and $R_2 = 0.152 R_{\odot}$. The vast majority of sdB stars are clustered near the canonical mass of $0.47 M_{\odot}$ (Fontaine et al. 2012), whereas the sdB mass in the binary system is unusually low. This paper is the fourth of a series of studies on the HW Vir-type systems (Lee et al. 2009a, 2014; Hong et al. 2017). We present the physical properties of 2M 1533+3759 from both the light-curve synthesis and the eclipse timing analysis, which are based on our new long-term observations.

2. NEW LONG-TERM CCD PHOTOMETRY

We took CCD photometric observations of 2M 1533+3759 for 76 nights from 2010 May through 2016 May, using the 1.0-m reflector at Mt. Lemmon Optical Astronomy Observatory (LOAO) in Arizona, USA. The observations of 2010 were made with a FLI IMG4301E 2K CCD camera, which

has 2084×2084 pixels and a field of view (FOV) of 22.2×22.2 arcmin². The observations of the other seasons were made with an ARC 4K CCD camera, which has 4096×4096 pixels and a FOV of 28×28 arcmin². We set up the 2×2 binning modes for both cameras and their readout times are about 14 s including pre-flushing. A summary of the observations is given in Table 1, where we present the observing intervals, number of nights, filters, typical exposure times, number of observed points, and number of primary and secondary eclipses. The instruments and reduction methods for the CCD cameras are the same as those described by Lee et al. (2009b, 2012).

In order to construct an artificial comparison star that would be optimal for the LOAO data, we monitored tens of stars imaged on the chip at the same time as 2M 1533+3759. Among them, four useful nearby stars were selected and combined by a weighted average. From all observing seasons, a total of 12,696 individual observations were obtained in the two bandpasses (3408 in *V* and 9288 in *I*), and a sample of them is listed in Table 2, where the times are Barycentric Julian Dates (BJD) in the Barycentric Dynamical Time system (Eastman et al. 2010). The differential magnitudes from the artificial reference star were computed and the resultant light curves are displayed in Figure 1. Each light curve is labeled with the observing season and filter used (e.g., 2010*V*).

3. LIGHT AND VELOCITY SOLUTIONS

As shown in Figure 1, the light curves of 2M 1533+3759 display sharp eclipses and strong reflection effects, which increase towards longer wavelengths. Nonetheless, there are no significant differences among the seven seasonal datasets. The depths of the primary and secondary eclipses are 1.35 mag and 0.12 mag in the *V* band, and 1.34 mag and 0.17 mag in the *I* band. In order to obtain a consistent set of the binary parameters, we simultaneously modeled our long-term photometric data and the single-lined RV curve of For et al. (2010) by using the 2007 version of the Wilson-Devinney synthesis code (Wilson & Devinney 1971; van Hamme & Wilson 2007; hereafter W-D). The light-curve synthesis was performed in a way similar to that of the sdB+M eclipsing system HW Vir (Lee et al. 2009a). The method of multiple subsets (Wilson & Biermann 1976) was used to determine the parameters and investigate our solution’s stability.

In our modeling, the surface temperature of the hot primary star was given as $T_1 = 29,230$ K from the spectroscopic analysis of For et al. (2010). The gravity-darkening exponents were assumed to be standard values of $g_1=1.0$ and $g_2=0.32$ (von Zeipel 1924; Lucy 1967), while the bolometric albedos were fixed at $A_1=A_2=1.0$ (Rucinski 1969a,b) because the cool secondary star is highly irradiated and heated by the sdB primary. The logarithmic bolometric (X, Y) and monochromatic (x, y) limb-darkening coefficients were initialized from the values of van Hamme (1993) in concert with the model atmosphere option. Furthermore, a synchronous rotation for both components was adopted and the detailed reflection effect was used (Wilson 1993). This synthesis was repeated until the correction of each free parameter became smaller than its standard error using the differential correction program of the W-D code. In this paper, the subscripts 1 and 2 refer to the sdB star

and its companion, respectively.

The mass ratio ($q=M_2/M_1$) is one of the most important parameters needed to understand the physical properties of binary systems. However, since there is still no spectroscopic mass ratio for 2M 1533+3759, we conducted a q -search procedure for a series of models with varying q between 0.22 and 0.35, which correspond to the sdB mass range from $\sim 0.30 M_\odot$ to $\sim 0.80 M_\odot$ theoretically predicted by Han et al. (2003). The q search was made simultaneously for all light and RV curves. In Figure 2, the weighted sum of the squared residuals ($\sum W(O - C)^2$; hereafter \sum) reached a global minimum at $q=0.28$, which was adopted as the initial value and thereafter adjusted to derive the binary parameters of the system. The final results are listed in the second and third columns of Table 3. We assumed that the temperatures of the primary and secondary components have the errors of 500 K and 600 K, respectively, following For et al. (2010). The synthetic VI light curves are displayed as solid lines in Figure 3 and the synthetic RV curves are plotted in Figure 4. In the figures, our binary model appears to fit the light and RV curves quite well. At this point, we considered an orbital eccentricity of the binary star as an adjustable parameter but found that the value remained zero. The result implies that the eclipsing binary has negligible eccentricity.

The consistent light and RV solution allows us to compute the absolute parameters of 2M 1533+3759 listed in Table 4, together with those of For et al. (2010) for comparison. The luminosity (L) and bolometric magnitudes (M_{bol}) were obtained by adopting the solar values of $T_{\text{eff}\odot} = 5,780$ K and $M_{\text{bol}\odot} = +4.73$. For the absolute visual magnitudes (M_V), we used the bolometric corrections (BCs) appropriate for the effective temperature of each component using the correlation between $\log T_{\text{eff}}$ and BC (Torres 2010). Most parameters are in accord with those of For et al. (2010) within the limits of their errors. The mass and surface gravity of the primary component presented in this paper are well matched with the canonical sdB value of $0.47 \pm 0.03 M_\odot$ (Fontaine et al. 2012) and the spectroscopic parameter of $\log g = 5.58 \pm 0.03$ (For et al. 2010), respectively. The physical parameters of the secondary star correspond to a spectral type of approximately M7V. These indicate that 2M 1533+3759 is a detached binary with the sdB primary star slightly larger than the M-type dwarf companion.

With an apparent visual magnitude of $V = +12.96 \pm 0.17$ (Kupfer et al. 2015) and the interstellar absorption of $A_V = 0.035$ (Schlafly & Finkbeiner 2011), we derived the distance of the system to be 524 ± 47 pc. Compared with the result of For et al. (2010), we obtained a slightly higher luminosity but placed the binary star at closer distance. This may be mainly caused by the values of V and A_V different from each other. For et al. (2010) appears to use $V = +13.61$ (Kelly & Shaw 2007) for a distance determination. Using their V magnitude and our values, the distance was calculated to be 707 ± 63 pc, which is consistent with that (644 ± 66 pc) of For et al. (2010) within the errors. On the other hand, considering the temperature error of the primary star, we performed the light-curve synthesis for 28,730 K and 29,730 K. The light and RV parameters from both values are in good agreement with those from $T_1 = 29,230$ K. We can see that the adopted T_1 does not affect the physical parameters presented in this paper.

Because the sdB primary component of 2M 1533+3759 lies at the boundary between both classes (V361 Hya and V1093 Her) of pulsating stars in the $T_{\text{eff}} - \log g$ diagram (Green et al. 2011), it could be a candidate for hybrid pulsators. Using the PERIOD04 program (Lenz & Breger 2005), we applied multiple frequency analyses to the light residuals from our binary models, but detected no pulsating periodicity with signal-to-noise amplitude ratios larger than 4.0 (Breger et al. 1993).

4. ECLIPSE TIMING VARIATION AND ITS IMPLICATIONS

From all our CCD observations, we determined 111 eclipse times and their errors using the method of Kwee & van Woerden (1956). These are listed in Table 5, wherein Min I and Min II represent the primary and secondary minima, respectively. In addition to our measurements, 266 CCD timings were collected from Drake et al. (2010), For et al. (2010), Zhu & Qian (2010), Backhaus et al. (2012), and Lohr et al. (2014). The HJD times based on UTC were transformed into TDB-based BJD ones using the online applets¹ developed by Eastman et al. (2010). For ephemeris computations, weights were calculated as the inverse squares of the timing errors.

The orbital period of 2M 1533+3759 has already been studied several times. Backhaus et al. (2012) and Lohr et al. (2014) reported that there is no clear evidence for the period change, while Zhu et al. (2015, 2016) suggested that a small amplitude cyclic variation may exist with a period of 7.6 yr, implying the presence of a Jupiter mass planet in the system. First of all, we introduced all eclipse times into a linear least-squares fit and thus found an improved ephemeris, as follows:

$$C = \text{BJD } 2,456,021.8529058(20) + 0.16177045211(32). \quad (1)$$

The parenthesized numbers are the 1σ -error values for the last digit of each ephemeris term. The eclipse timing $O-C$ diagram constructed with equation (1) is plotted in the upper panel of Figure 5, where the blue and red circles are the primary and secondary eclipses, respectively. To see if the eclipse timings represent a real and periodic variation, we applied a periodogram analysis to the timing residuals, but no credible periodicity was found. Moreover, because recent timings appear to display a period decrease, we fitted the minimum epochs to a parabolic ephemeris. The result indicated that the quadratic term is not significant. Thus, the orbital period of the binary system can be considered constant.

In Figure 5, the primary and secondary timing residuals seem not to agree with each other. In order to examine this discrepancy in detail, we computed the secondary eclipse times related to one half period after the primary eclipse times and then plotted the difference (Δt_{SE}) between the observed and computed times of the secondary eclipses in the lower panel of Figure 5. As can be seen from the figure, the secondary times shifted from zero by the mean value of $\Delta t_{\text{SE}} = 3.9 \pm 1.0$ s. The time difference between both eclipses could be caused by the Rømer delay (Δt_{Rd}) in the

¹<http://astrutils.astronomy.ohio-state.edu/time/>

binary star with a mass ratio far from unity (Kaplan 2010; Lee et al. 2017):

$$\Delta t_{\text{Rd}} = \frac{PK_1}{\pi c} \left(\frac{1}{q} - 1 \right), \quad (2)$$

where P is the binary period, K_1 is the sdB velocity semi-amplitude, c is the speed of light, and q is the mass ratio. Using the parameters in Table 3, we got a time delay of $\Delta t_{\text{Rd}} = 2.7 \pm 1.4$ s, which is in good agreement with the observed delay of Δt_{SE} in the arrival times of the secondary eclipses relative to the the primary eclipses.

Although 2M 1533+3759 has negligible eccentricity (e), it does not mean that the eclipsing system is in a circular orbit. Even in a case that the binary’s orbit has a very small eccentricity, the observed delay of Δt_{SE} could be affected by the time shift of Δt_e in the secondary eclipse due to non-zero eccentricity:

$$\Delta t_e \simeq \frac{2Pe}{\pi} \cos \omega = \Delta t_{\text{SE}} - \Delta t_{\text{Rd}}, \quad (3)$$

where ω is the argument of periastron. Using the equation (3), the orbital eccentricity of 2M 1533+3759 is calculated to be $e \cos \omega \simeq 0.0001$. If Δt_{SE} is fully produced by an eccentricity, $e \cos \omega \simeq 0.0004$.

Finally, we added the time shift of $\Delta t_{\text{SE}} = 3.9$ s to the secondary eclipses and then applied a linear least-squares fit to all minimum times as before. As a result, the reference epoch and period of the new ephemeris are calculated to be BJD 2,456,021.8529060 and 0.16177045212 d, respectively, which are essentially identical to those given in equation (1). This is because the root-mean-square (rms) scatter (~ 10 s) of the timing measurements is about 2.5 times larger than the observed time delay in the secondary eclipses.

5. DISCUSSION AND CONCLUSIONS

In this paper, we presented new CCD photometry of 2M 1533+3759 made for seven years from 2010 to 2016. The VI light curves, which display sharp eclipses and prominent reflection effects, were solved simultaneously with the single-lined RV curve of For et al. (2010). Our light and velocity solutions represent that the eclipsing pair is a HW Vir-type detached binary with a mass ratio of $q = 0.280$, an orbital inclination of $i = 86.80$ deg, and a temperature ratio between the components of $T_2/T_1 = 0.106$. The primary and secondary components fill $f_1 = 39$ % and $f_2 = 76$ % of their limiting lobe, respectively, where the filling factor $f_{1,2} = \Omega_{\text{in}}/\Omega_{1,2}$. The masses and radii of both components are determined to be $M_1 = 0.442 M_\odot$, $M_2 = 0.124 M_\odot$, $R_1 = 0.172 R_\odot$, and $R_2 = 0.157 R_\odot$. These indicate that the primary is typical for a normal sdB star and the secondary is an M7 main sequence star.

The eclipse times of 2M 1533+3759, spanning about 12 yrs, have been examined and they indicate that the orbital period has been essentially constant. From the time difference between

both types of minima, we measured a delay of 3.9 ± 1.0 s in the arrival times of the secondary eclipses relative to the primary eclipses. The observed value is in satisfactory accord with the expected Rømer delay of 2.7 ± 1.4 s across the binary orbit. This indicates that the Rømer delay is the main cause of the time shift in the secondary eclipses measured in this paper, which is the second detection in HW Vir-type binaries (Barlow et al. 2012). Nonetheless, the time delay of the secondary eclipse may come from both the Rømer delay and the non-zero eccentricity. Our result limits the eccentricity of 2M 1533+3759 to $e \leq 0.0001$. Because the predicted Rømer delay is less than ~ 3 s, future timing measurements with accuracies better than the value will help to reveal more detailed properties of the binary star.

The authors wish to thank the staff of LOAO for assistance during our observations. We appreciate the careful reading and valuable comments of the anonymous referee. This research has made use of the Simbad database maintained at CDS, Strasbourg, France, and was supported by the KASI grant 2017-1-830-03. The work by K. Hong and W. Han was supported by grant numbers NRF-2016R1A6A3A01007139 and NRF-2014M1A3A3A02034746 of the National Research Foundation of Korea (NRF), respectively.

REFERENCES

- Barlow, B. N., Wade, R. A., & Liss, S. E. 2012, *ApJ*, 753, 101
- Backhaus, U., Bauer, S., Beuermann, K., et al. 2012, *A&A*, 538, A84
- Breger, M., Stich, J., Garrido, R., et al. 1993, *A&A*, 271, 482
- Copperwheat, C. M., Morales-Rueda, L., Marsh, T. R., Maxted, P. F. L., & Heber, U. 2011, *MNRAS*, 415, 138
- Drake, A. J., Beshore, E., Catelan, M., et al. 2010, arXiv:1009.3048
- Eastman, J., Siverd, R., & Gaudi, B. S. 2010, *PASP*, 122, 935
- Fontaine, G., Brassard, P., Charpinet, S., et al. 2012, *A&A*, 539, A12
- For, B.-Q., Green, E. M., Fontaine, G., et al. 2010, *ApJ*, 708, 253
- Green, E. M., Guvenen, B., O’Malley, C. J., et al. 2011, *ApJ*, 734, 59
- Han, Z., Podsiadlowski, P., Maxted, P. F. L., & Marsh, T. R. 2003, *MNRAS*, 341, 669
- Heber, U. 2016, *PASP*, 128, 2001
- Hong, K., Lee, J. W., Kim, S.-L., et al. 2017, *PASP*, 129, 4202
- Irwin, J. B. 1952, *ApJ*, 116, 211
- Irwin, J. B. 1959, *AJ*, 64, 149
- Kaplan, D. L. 2010, *ApJ*, 717, L108
- Kelley, N., & Shaw, J. S. 2007, *J. Southeastern Assoc. Res. Astron.*, 1, 13
- Kreiner, J. M., Kim, C.-H., & Nha, I.-S. 2001, *An Atlas of $O-C$ Diagrams of Eclipsing Binary Stars* (Krakow: Wydawn. Nauk. Akad. Pedagogicznej)
- Kupfer, T., Geier, S., Heber, U., et al. 2015, *A&A*, 576, A44
- Kwee, K. K., & van Woerden, H. 1956, *Bull. Astron. Inst. Netherlands*, 12, 327
- Lee, J. W., Hinse, T. C., Youn, J.-H., & Han, W. 2014, *MNRAS*, 445, 2331
- Lee, J. W., Hong, K., Kim, S.-L., & Koo, J.-R. 2017, *ApJ*, 835, 189
- Lee, J. W., Kim, S.-L., Kim, C.-H., et al. 2009a, *AJ*, 137, 3181
- Lee, J. W., Youn, J.-H., Kim, S.-L., Lee, C.-U., & Hinse, T. C. 2012, *AJ*, 143, 95

- Lee, J. W., Youn, J.-H., Lee, C.-U., Kim, S.-L., & Koch, R. H. 2009b, *AJ*, 138, 478
- Lenz, P., & Breger, M. 2005, *Comm. Asteroseismology*, 146, 53
- Lohr, M. E., Norton, A. J., Anderson, D. R., et al. 2014, *A&A*, 566, A128
- Lucy, L. B. 1967, *Z. Astrophys.*, 65, 89
- Maxted, P. F. L., Heber, U., Marsh, T. R., & North, R. C. 2001, *MNRAS*, 326, 1391
- Mochnecki, S. W. 1984, *ApJS*, 55, 551
- Paczynski, B. 1976, in *IAU Symp. 73, Structure and Evolution of Close Binary Systems*, ed. P. Eggleton, S. Mitton, & J. Whelan (Dordrecht: D. Reidel), 75
- Ribas, I. 2006, in *ASP Conf. Ser. 349, Astrophysics of Variable Stars*, ed. C. Sterken & C. Aerts (San Francisco: ASP), 55
- Rucinski, S. M. 1969a, *Acta. Astron.*, 19, 125
- Rucinski, S. M. 1969b, *Acta. Astron.*, 19, 245
- Schlafly, E. F., & Finkbeiner, D. P. 2011, *AJ*, 737, 103
- Torres, G. 2010, *AJ*, 140, 1158
- Van Hamme, W. 1993, *AJ*, 106, 209
- Van Hamme, W., & Wilson, R. E. 2007, *ApJ*, 661, 1129
- Von Zeipel, H., 1924, *MNRAS*, 84, 665
- Wilson, R. E. 1993, in *ASP Conf. Ser. 38, New Frontiers in Binary Star Research*, ed. K.-C. Leung & I.-S. Nha (San Francisco, CA: ASP), 91
- Wilson, R. E., & Biermann, P. 1976, *A&A*, 48, 349
- Wilson, R. E., & Devinney, E. J. 1971, *ApJ*, 166, 605
- Zhu, L. Y., & Qian, S. B. 2010, *Ap&SS*, 329, 107
- Zhu, L. Y., Qian, S. B., Liao, W. P., et al. 2015, *Publ. Korean Astron. Soc.*, 30, 289
- Zhu, L. Y., Qian, S. B., Liao, W. P., Zhao, E., & Li, L. 2016, *J. Phys. Conf. Ser.* 728, 072023
- Zorotovic, M., & Schreiber, M. R. 2013, *A&A*, 549, 95

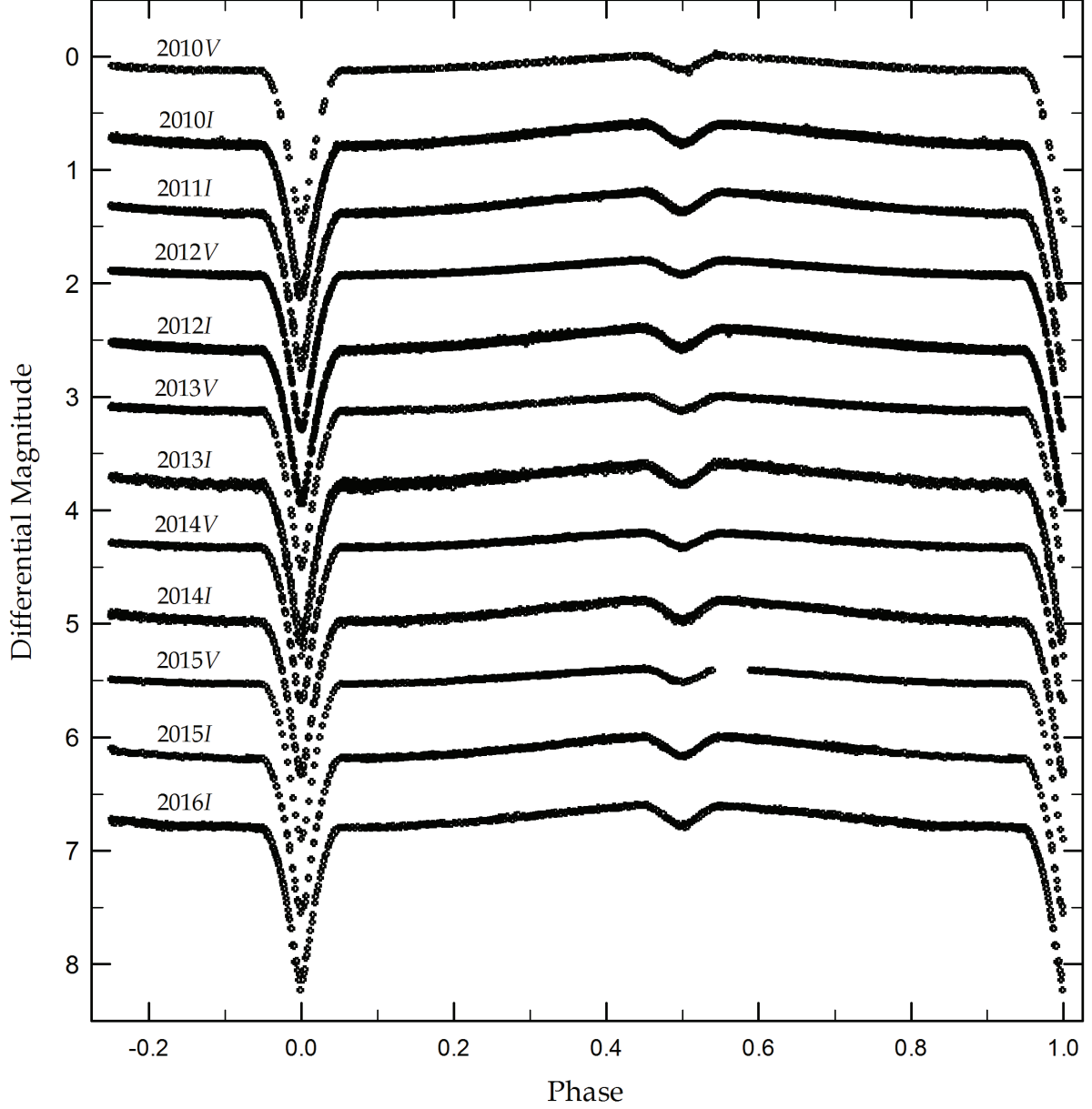


Fig. 1.— Light curves of 2M 1533+3759 obtained from 2010 to 2016 in *VI* bandpasses. All but 2010V are displaced vertically for clarity.

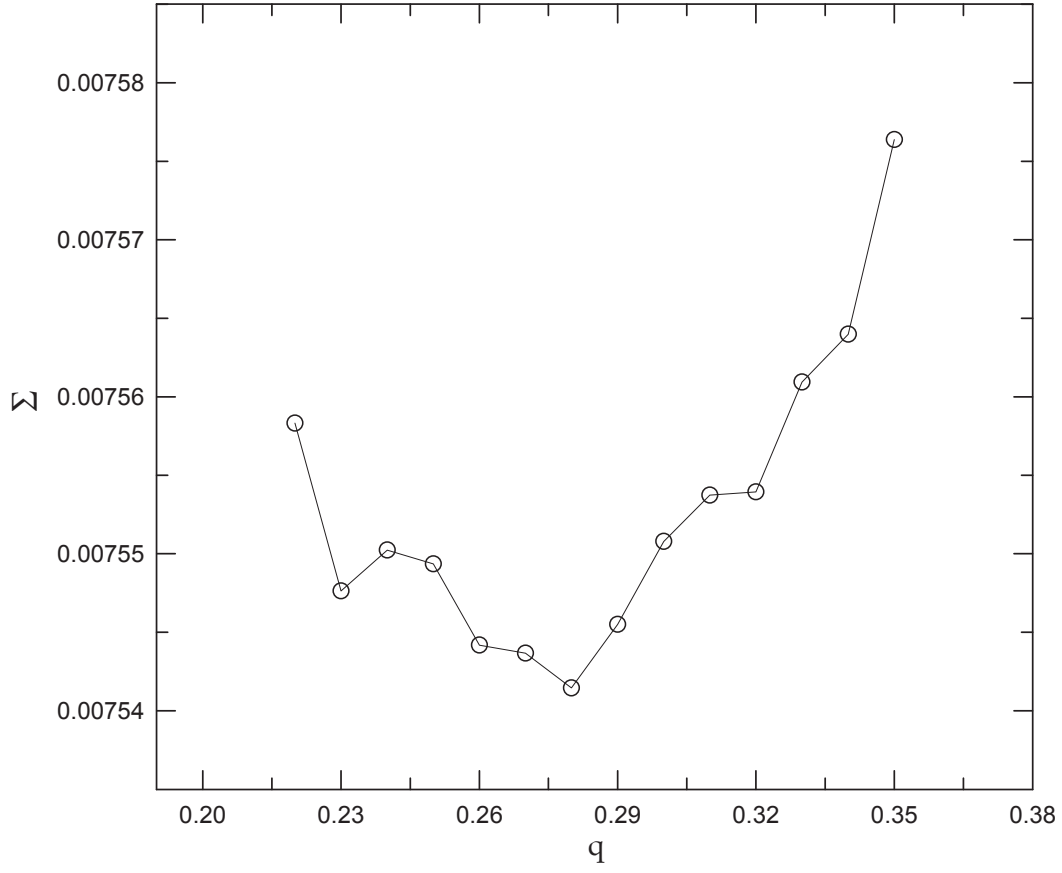


Fig. 2.— Behavior of \sum of 2M 1533+3759 as a function of mass ratio q , showing a global minimum at $q=0.28$.

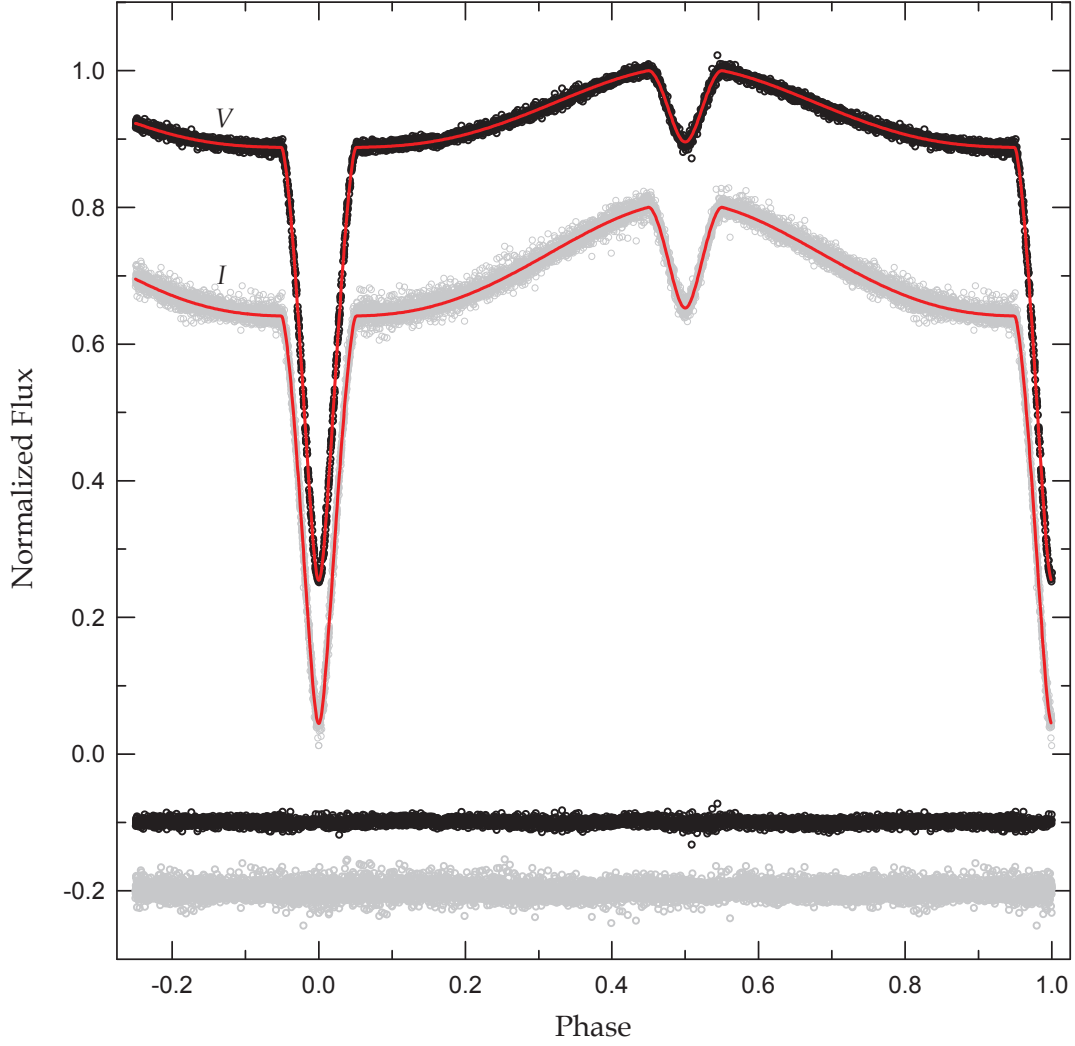


Fig. 3.— Normalized V (black circle) and I (gray circle) light curves with fitted models. The red solid curves are computed with the model parameters of Table 3. The corresponding residuals from the fits are offset from zero and plotted at the bottom in the same order as the light curves.

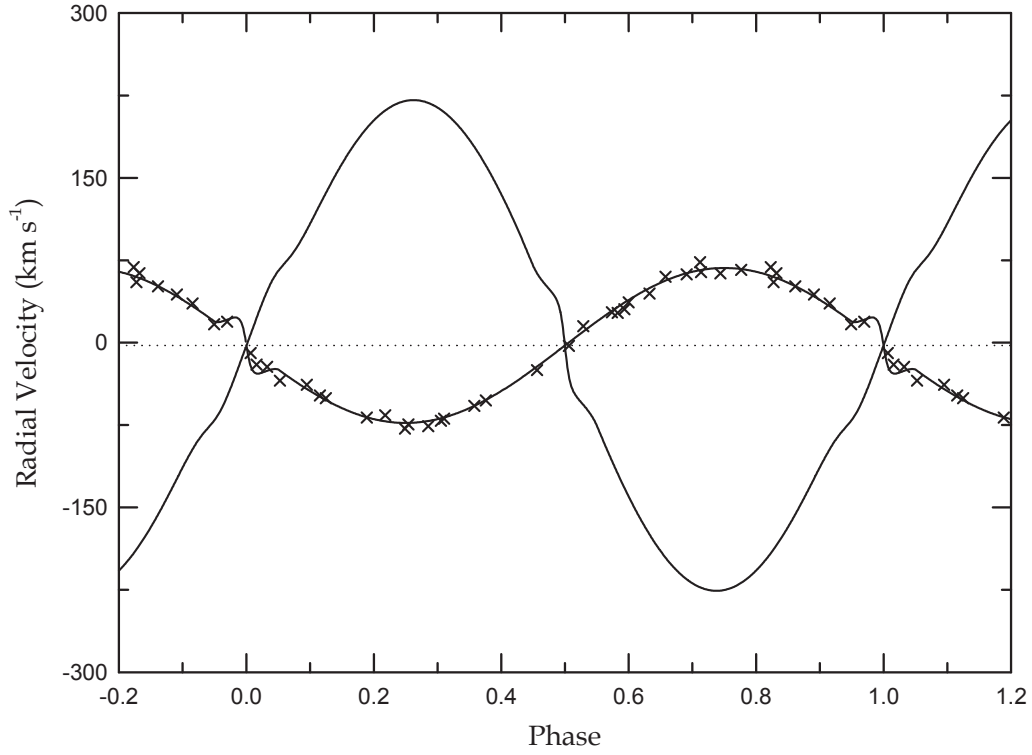


Fig. 4.— Radial-velocity curves of 2M 1533+3759. The ‘x’ symbols are the measurements of For et al. (2010), while the solid curves denote the result from consistent light and RV curve analysis. The dotted line refers to the systemic velocity of -2.5 km s^{-1} .

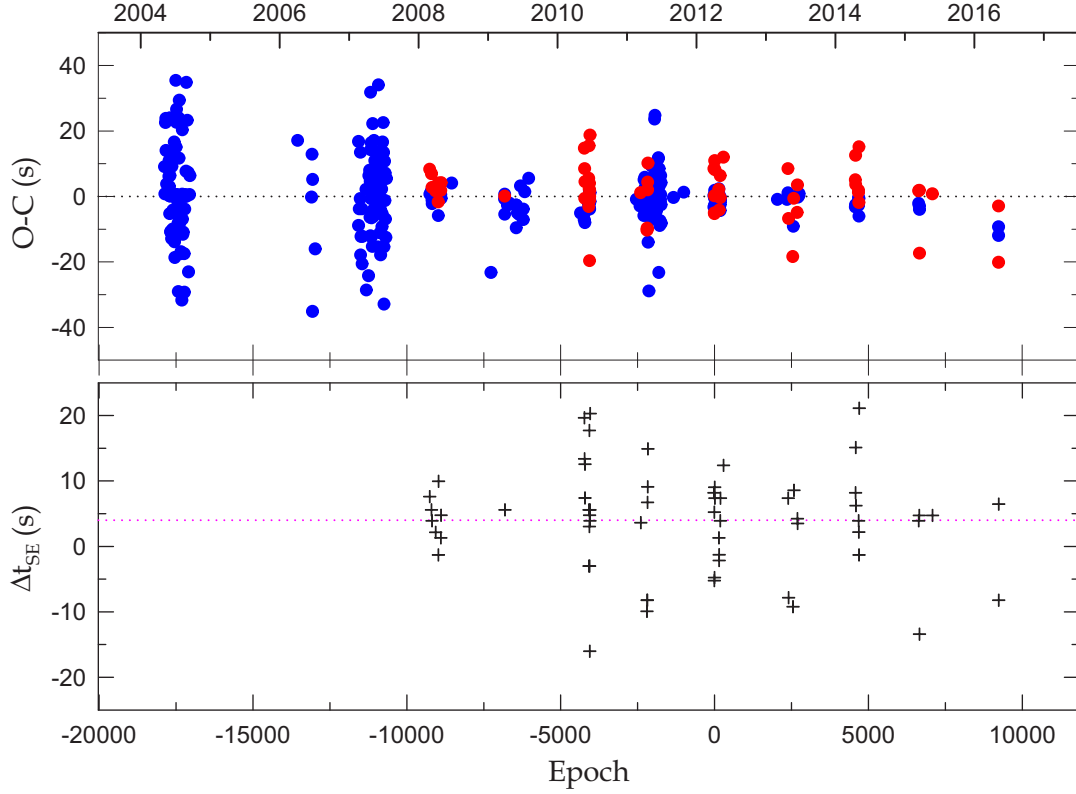


Fig. 5.— The upper panel shows the eclipse timing diagram of 2M 1533+3759 constructed with the linear ephemeris of equation (1). The blue and red circles represent the primary and secondary minima, respectively. The lower panel displays the time delay (Δt_{SE}) of the secondary eclipses related to one half period after the primary eclipse times. The dotted line refers to the mean value of $\Delta t_{SE} = 3.9$ s.

Table 1. Observing log of 2M 1533+3759.

Season	Observing Interval	N_{night}	Filter	Exp. Time (s)	N_{obs}	$N_{\text{MinI/MinII}}$
2010	May 01–June 19	12	<i>VI</i>	70	2502	16/14
2011	March 10–April 20	12	<i>I</i>	55	1463	7/7
2012	March 30–May 22	20	<i>VI</i>	70	3104	16/12
2013	March 01–June 24	19	<i>VI</i>	45	2073	9/6
2014	April 15–May 04	7	<i>VI</i>	35	1929	6/7
2015	March 13–May 24	5	<i>VI</i>	35	1016	3/4
2016	May 06	1	<i>I</i>	35	609	2/2

Table 2. CCD photometric observations of 2M 1533+3759.

BJD	ΔV (mag)	BJD	ΔI (mag)
2,455,360.65054	0.0684	2,455,317.93713	0.0675
2,455,360.65244	0.0712	2,455,317.93929	0.0699
2,455,360.65432	0.0792	2,455,317.94036	0.0731
2,455,360.65621	0.0851	2,455,317.94144	0.0834
2,455,360.65810	0.0945	2,455,317.94246	0.0863
2,455,360.65998	0.0986	2,455,317.94342	0.0942
2,455,360.66187	0.1000	2,455,317.94438	0.0944
2,455,360.66377	0.1008	2,455,317.94534	0.1032
2,455,360.66565	0.1114	2,455,317.94630	0.0956
2,455,360.66754	0.1101	2,455,317.94726	0.1118

Note. — This table is available in its entirety in machine-readable form.

Table 3. Velocity and light curve parameters of 2M 1533+3759.

Parameter	Primary	Secondary
T_0 (HJD)	2,456,021.8528710±0.0000076	
P (day)	0.1617704495±0.0000000021	
a (R_\odot)	1.033±0.017	
γ (km s^{-1})	−2.5±1.1	
K_1 (km s^{-1})	70.6±2.1	
K_2 (km s^{-1})	252.0±3.2	
q	0.2802±0.0049	
i (deg)	86.802±0.066	
T (K)	29230±500	3089±600
Ω	6.289±0.044	3.208±0.010
Ω_{in}	2.422	
X, Y	0.762, 0.255	0.463, 0.290
x_V, y_V	0.334±0.043, 0.210	0.855±0.084, 0.361
x_I, y_I	0.261±0.058, 0.164	0.748±0.073, 0.352
$L/(L_1 + L_2)_V$	0.9998±0.0002	0.0002±0.0001
$L/(L_1 + L_2)_I$	0.9976±0.0005	0.0024±0.0004
r (pole)	0.1663±0.0012	0.1507±0.0006
r (point)	0.1672±0.0012	0.1553±0.0007
r (side)	0.1668±0.0012	0.1519±0.0006
r (back)	0.1671±0.0012	0.1546±0.0006
r (volume) ^a	0.1668±0.0012	0.1525±0.0006

^aMean volume radius computed from the tables given by Mochnacki (1984).

Table 4. Absolute parameters for 2M 1533+3759.

Parameter	For et al. (2010)		This Work	
	Primary	Secondary	Primary	Secondary
M (M_{\odot})	0.376 ± 0.055	0.113 ± 0.017	0.442 ± 0.012	0.124 ± 0.005
R (R_{\odot})	0.166 ± 0.007	0.152 ± 0.005	0.172 ± 0.002	0.157 ± 0.002
$\log g$ (cgs)	5.58 ± 0.03	...	5.61 ± 0.02	5.14 ± 0.02
L (L_{\odot})	18.14 ± 1.84	...	19.4 ± 1.4	0.002 ± 0.002
M_{bol} (mag)	$+1.51 \pm 0.08$	$+11.47 \pm 0.84$
BC (mag)	-2.82 ± 0.05	-4.36 ± 4.71
M_V (mag)	$+4.57 \pm 0.21$...	$+4.33 \pm 0.09$	$+15.83 \pm 4.78$
Distance (pc)	644 ± 66		524 ± 47	

Table 5. New times of minimum light for 2M 1533+3759.

BJD (2,450,000+)	Error	Filter	Min	BJD (2,450,000+)	Error	Filter	Min
5317.98961	± 0.00002	<i>I</i>	I	6044.74345	± 0.00003	<i>V</i>	II
5336.91673	± 0.00002	<i>I</i>	I	6044.82432	± 0.00002	<i>V</i>	I
5337.96849	± 0.00003	<i>I</i>	II	6045.71405	± 0.00005	<i>I</i>	II
5338.85800	± 0.00002	<i>I</i>	I	6045.79496	± 0.00001	<i>I</i>	I
5338.93904	± 0.00004	<i>I</i>	II	6045.87577	± 0.00005	<i>I</i>	II
5340.71841	± 0.00006	<i>I</i>	II	6045.95667	± 0.00002	<i>I</i>	I
5340.88024	± 0.00004	<i>I</i>	II	6046.76555	± 0.00001	<i>V</i>	I
5340.96098	± 0.00002	<i>I</i>	I	6046.92729	± 0.00002	<i>V</i>	I
5359.88820	± 0.00002	<i>I</i>	I	6051.78041	± 0.00001	<i>I</i>	I
5360.69704	± 0.00007	<i>V</i>	I	6051.86132	± 0.00004	<i>I</i>	II
5360.85882	± 0.00007	<i>V</i>	I	6051.94216	± 0.00003	<i>I</i>	I
5361.74854	± 0.00005	<i>I</i>	II	6052.75104	± 0.00001	<i>V</i>	I
5361.82946	± 0.00002	<i>I</i>	I	6052.83202	± 0.00009	<i>V</i>	II
5361.91041	± 0.00008	<i>I</i>	II	6052.91282	± 0.00001	<i>V</i>	I
5363.69000	± 0.00007	<i>I</i>	II	6053.88345	± 0.00001	<i>I</i>	I
5363.77068	± 0.00002	<i>I</i>	I	6068.84736	± 0.00006	<i>I</i>	II
5363.85162	± 0.00005	<i>I</i>	II	6352.99701	± 0.00002	<i>I</i>	I
5363.93247	± 0.00001	<i>I</i>	I	6402.98408	± 0.00001	<i>V</i>	I
5364.66049	± 0.00005	<i>I</i>	II	6408.80783	± 0.00002	<i>I</i>	I
5364.74132	± 0.00001	<i>I</i>	I	6408.88881	± 0.00008	<i>I</i>	II
5364.82220	± 0.00004	<i>I</i>	II	6408.96961	± 0.00003	<i>I</i>	I
5364.90312	± 0.00001	<i>I</i>	I	6410.99165	± 0.00008	<i>V</i>	II
5365.71191	± 0.00003	<i>V</i>	I	6433.96292	± 0.00005	<i>I</i>	II
5365.79261	± 0.00007	<i>V</i>	II	6436.95578	± 0.00005	<i>I</i>	I
5366.76346	± 0.00007	<i>V</i>	II	6438.97801	± 0.00008	<i>I</i>	II
5366.84430	± 0.00003	<i>V</i>	I	6456.93448	± 0.00007	<i>I</i>	II
5366.92525	± 0.00007	<i>V</i>	II	6457.90520	± 0.00007	<i>V</i>	II
5367.65321	± 0.00003	<i>I</i>	I	6459.92729	± 0.00001	<i>V</i>	I
5367.81495	± 0.00002	<i>I</i>	I	6460.89791	± 0.00003	<i>I</i>	I
5367.89607	± 0.00007	<i>I</i>	II	6465.91280	± 0.00005	<i>I</i>	I
5631.01546	± 0.00001	<i>I</i>	I	6466.88343	± 0.00002	<i>I</i>	I
5632.95671	± 0.00002	<i>I</i>	I	6762.92331	± 0.00002	<i>I</i>	I

Table 5—Continued

BJD (2,450,000+)	Error	Filter	Min	BJD (2,450,000+)	Error	Filter	Min
5634.00826	± 0.00006	<i>I</i>	II	6763.00429	± 0.00007	<i>I</i>	II
5662.88427	± 0.00001	<i>I</i>	I	6763.89394	± 0.00001	<i>V</i>	I
5666.84753	± 0.00005	<i>I</i>	II	6763.97500	± 0.00010	<i>V</i>	II
5666.92853	± 0.00002	<i>I</i>	I	6764.94552	± 0.00006	<i>I</i>	II
5667.89914	± 0.00002	<i>I</i>	I	6778.85775	± 0.00003	<i>V</i>	II
5667.97993	± 0.00003	<i>I</i>	II	6778.93859	± 0.00001	<i>V</i>	I
5668.86976	± 0.00001	<i>I</i>	I	6779.82838	± 0.00004	<i>I</i>	II
5668.95055	± 0.00006	<i>I</i>	II	6779.90924	± 0.00001	<i>I</i>	I
5669.92131	± 0.00003	<i>I</i>	II	6780.87986	± 0.00001	<i>V</i>	I
5670.89196	± 0.00003	<i>I</i>	II	6780.96073	± 0.00003	<i>V</i>	II
5670.97274	± 0.00001	<i>I</i>	I	6781.85042	± 0.00001	<i>I</i>	I
5671.86265	± 0.00006	<i>I</i>	II	6781.93155	± 0.00006	<i>I</i>	II
6018.77927	± 0.00003	<i>V</i>	I	7094.95722	± 0.00005	<i>I</i>	II
6018.86025	± 0.00007	<i>V</i>	II	7095.03806	± 0.00002	<i>I</i>	I
6018.94100	± 0.00003	<i>V</i>	I	7097.94992	± 0.00001	<i>V</i>	I
6020.80140	± 0.00007	<i>I</i>	II	7098.03086	± 0.00007	<i>V</i>	II
6020.96311	± 0.00003	<i>I</i>	II	7098.92053	± 0.00001	<i>I</i>	I
6021.85290	± 0.00002	<i>I</i>	I	7099.00126	± 0.00009	<i>I</i>	II
6021.93373	± 0.00004	<i>I</i>	II	7166.94506	± 0.00004	<i>I</i>	II
6022.82355	± 0.00002	<i>I</i>	I	7514.67050	± 0.00002	<i>I</i>	I
6022.90454	± 0.00006	<i>I</i>	II	7514.75129	± 0.00007	<i>I</i>	II
6022.98527	± 0.00001	<i>I</i>	I	7514.83230	± 0.00001	<i>I</i>	I
6023.87513	± 0.00003	<i>V</i>	II	7514.91326	± 0.00006	<i>I</i>	II
6023.95593	± 0.00001	<i>V</i>	I				